Solution-processed PbS quantum dot infrared photodetectors and photovoltaics

STEVEN A. MCDONALD[1], GERASIMOS KONSTANTATOS[1], SHIGUO ZHANG[1], PAUL W. CYR[1,2], ETHAN J. D. KLEM[1], LARISSA LEVINA[1] AND EDWARD H. SARGENT[1]*

[1]Department of Electrical and Computer Engineering, University of Toronto, Toronto, Ontario, M5S 3G4, Canada

[2]Department of Chemistry, University of Toronto, Toronto, Ontario, M5S 3H6, Canada

*e-mail: ted.sargent@utoronto.ca

Published online: 9 January 2005; doi:10.1038/nmat1299

In contrast to traditional semiconductors, conjugated polymers provide ease of processing, low cost, physical flexibility and large area coverage[1]. These active optoelectronic materials produce and harvest light efficiently in the visible spectrum. The same functions are required in the infrared for telecommunications (1,300–1,600 nm), thermal imaging (1,500 nm and beyond), biological imaging (transparent tissue windows at 800 nm and 1,100 nm), thermal photovoltaics (>1,900 nm), and solar cells (800–2,000 nm). Photoconductive polymer devices have yet to demonstrate sensitivity beyond ~800 nm (refs 2,3). Sensitizing conjugated polymers with infrared-active nanocrystal quantum dots provides a spectrally tunable means of accessing the infrared while maintaining the advantageous properties of polymers. Here we use such a nanocomposite approach in which PbS nanocrystals tuned by the quantum size effect sensitize the conjugated polymer poly[2-methoxy-5-(2′-ethylhexyloxy-*p*-phenylenevinylene)] (MEH-PPV) into the infrared. We achieve, in a solution-processed device and with sensitivity far beyond 800 nm, harvesting of infrared-photogenerated carriers and the demonstration of an infrared photovoltaic effect. We also make use of the wavelength tunability afforded by the nanocrystals to show photocurrent spectra tailored to three different regions of the infrared spectrum.

Organic/nanocrystal composites have been demonstrated to enable a number of important optoelectronic devices operating in the visible region[4–8]. In the infrared, electroluminescence has been demonstrated from such materials[9–11]. In the area of infrared photodetection using nanocomposites there is one report with a low internal quantum efficiency of 10^{-5} at 5 V bias that necessitated the use of modulated illumination and a lock-in amplifier to observe the photocurrent[12]. Thus far, there has been no demonstration of an infrared photovoltaic effect from such a material system.

We demonstrate, using solution-processed materials, both a three-order-of-magnitude improvement in infrared photoconductive internal quantum efficiency compared with previous results[12], allowing observation of the photocurrent under continuous-wave illumination without reliance on lock-in techniques; and also the first observation of an infrared photovoltaic effect in such materials. Under –5 V bias and illumination from a 975 nm laser, our detectors show an internal quantum efficiency of 3%, a ratio of photocurrent to dark current of 630, and a maximum responsivity of 3.1×10^{-3} A W^{-1}. The photovoltaic response under 975 nm excitation results in a maximum open-circuit voltage of 0.36 V, short-circuit current of 350 nA, and short-circuit internal quantum efficiency of 0.006%. We also demonstrate, by varying the size of the nanocrystals during processing, photocurrent spectra with peaks tailored to 980 nm, 1.200 μm and 1.355 μm.

Quantum dot nanocrystals of PbS were chosen for their ability to sensitize MEH-PPV, which on its own absorbs between ~400 nm and ~600 nm, into the infrared. Our nanocrystals have absorption peaks tunable from ~800 nm to ~2,000 nm (ref. 13). We show herein that our devices' photocurrent spectrum corresponds to the nanocrystals' absorption spectrum, indicating that the sensitivity of the nanocomposite could potentially be tuned across the 800–2,000 nm spectral region.

The selection of the semiconducting polymer is critical to achieving charge separation between the nanocrystal and polymer. Conjugated polymers typically have better hole than electron mobility. Thus, photoconductivity in polymer/nanocrystal composites requires a band alignment that favours transfer of the photogenerated hole to the polymer; that is, the ionization potential of the polymer should, ideally, lie closer to vacuum than that of the nanocrystal. The bulk ionization potential of PbS is ~4.95 eV, whereas most conjugated polymers have ionization potentials greater than ~5.3 eV (ref. 14). The low ionization potential of PbS relative to other semiconductor materials used in nanocrystal-based photoconductive devices, such as the cadmium chalcogenides (bulk ionization potentials between ~6.4 eV and ~7.3 eV), limits the number of readily available conjugated polymers that provide a favourable energy alignment. MEH-PPV was selected for its low ionization potential, variously reported[15,16] between ~4.9 eV and ~5.1 eV. It was not obvious at the outset that MEH-PPV/PbS would provide the type-II heterojunction needed for efficient photoconduction and for the observation of a photovoltaic effect. The vacuum-referenced band edge of the organic component is uncertain; it is possible that a dipole layer could be formed at the

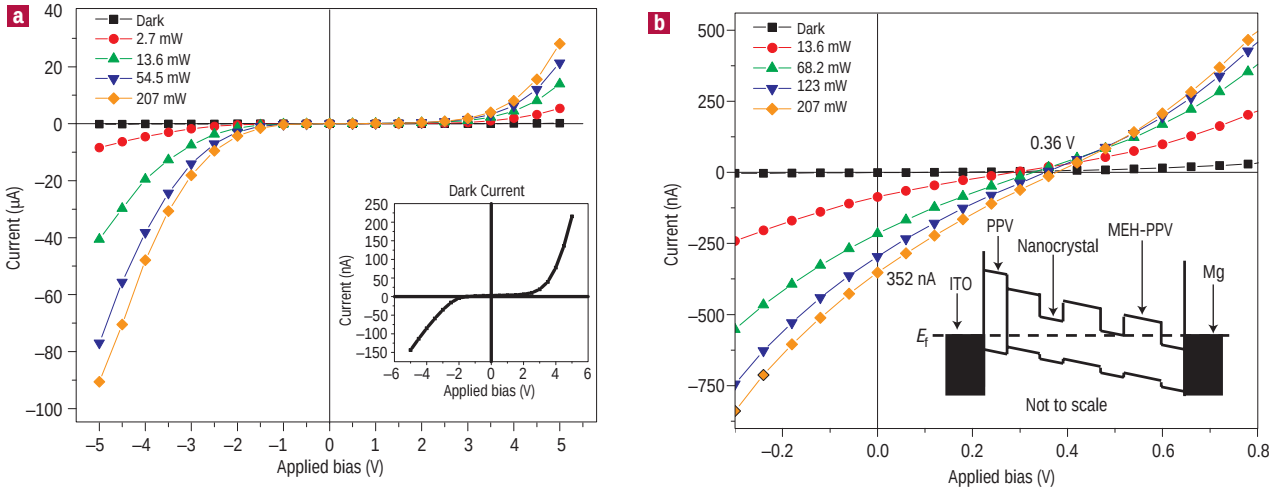

Figure 1 **Dark current and photocurrent versus applied bias at the ITO electrode**. The pump powers are shown in the key. **a**, Main panel: dark current and photocurrent results for a sample with ~90% by weight nanocrystals in the polymer/nanocrystal blend. Inset: dark current for the main panel. **b**, Main panel: dark current and photocurrent curves near zero bias, demonstrating the photovoltaic effect; these data were obtained from a different sample from that shown in **a** and represent the best results so far for short-circuit current and open-circuit voltage. Inset: proposed simplified band diagram depicting the relative energy alignments after the magnesium electrode has been deposited and the sample has reached equilibrium.

interface between materials, altering the effective band alignment; and the nanocrystal energy levels vary with size. However, MEH-PPV was one available conjugated polymer candidate to provide the correct heterostructure for this application.

The devices consist of a sandwich structure of glass, indium tin oxide (ITO), poly(*p*-phenylenevinylene) (PPV), MEH-PPV/PbS nanocrystal blend, and an upper magnesium contact. In addition to acting as a hole transport layer, the PPV layer provides a number of improvements over samples with the MEH-PPV/nanocrystal layer deposited directly on the ITO: it provides better electrical stability by forming a smooth and pinhole-free pre-layer on which the blend films can be cast, eliminating catastrophic shorts from the upper contact directly through to the ITO; it decreases the dark current by introducing an injection barrier at the ITO contact, allowing larger ratios of photocurrent to dark current; and it permits a higher bias to be applied to the samples before electrical breakdown, allowing the establishment of a higher internal field, more efficient photogenerated carrier extraction and consequently higher photocurrents. The PPV layer slightly reduces the photocurrent internal quantum efficiency because it also poses a barrier to the extraction of both photogenerated holes in the reverse bias and photogenerated electrons in the forward bias (it will be shown below that the barrier to extracting holes from the active region is less than that for electrons, resulting in higher photocurrent in the reverse bias). However, the PPV layer poses less of an extraction barrier than it does an injection barrier, which allows for the improved ratio of photocurrent to dark current. The slight reduction in efficiency was a compromise to obtain low dark current and to maximize the on/off ratio, of critical importance in detection and imaging applications.

The dark current and photocurrent are shown as a function of bias applied at the ITO electrode in Fig. 1a. The data were taken using an Agilent 4155C Semiconductor Parameter Analyzer and microprobe station. The optical excitation was provided by a 975 nm continuous-wave semiconductor laser, which allowed selective excitation of the nanocrystal phase. The dark current is 216 nA at a bias of 5 V and 144 nA at –5 V (inset, Fig. 1a). The photocurrent *I*–*V* curves show diode-like behaviour, with higher photocurrents in the reverse bias. At a bias of –5 V, the photocurrent is 8.43 μA for 2.7 mW incident power and 90.61 μA for 207 mW incident power, which represents a ratio of photocurrent to dark current of 59 and 630, respectively. The above photocurrent under 2.7 mW illumination represents a responsivity of 3.1×10^{-3} A W^{-1}. When ITO is positively biased at 5 V, the photocurrent is reduced to 5.39 and 28.12 μA for incident powers of 2.7 and 207 mW, respectively.

The asymmetry of the photocurrent *I*–*V* curves can be ascribed to the work-function difference between ITO (~4.8 eV) and magnesium (3.7 eV) and to the energy levels of the PPV layer. The inset of Fig. 1b shows a possible band diagram for the structure after the magnesium contact has been deposited and the device has reached the equilibrium state. For this diagram, the lowest-energy absorption peak is assumed to be the first excitonic absorption of the PbS nanocrystals. This is used to estimate an increase in bandgap energy relative to bulk PbS, which has a bandgap of 0.41 eV; for the nanocrystals with absorption peaks centred at 955, 1,200 and 1,355 nm (depicted in Fig. 3), the effective bandgaps are 1.30, 1.03 and 0.92 eV, respectively. Because of the nearly equal effective masses for holes and electrons in PbS, it is also assumed that the confinement energy is shared equally in the conduction and valence bands so the bands move up and down, respectively, by equal energies. The barrier for electrons comes from the octylamine ligand, which passivates the nanocrystal surface, and/or the MEH-PPV (ionization energy ~4.9 eV and electron affinity ~2.9 eV; ref. 15), that surrounds the nanocrystal. To align the Fermi level in all layers, the magnesium side tilts down and the ITO side tilts up. (Similar band tilting in polymers[17] and in C_{60}-doped polymers sandwiched between two different conductors[18] have been discussed previously.) After an electron in the valence band of the nanocrystal is transferred to the conduction band by absorbing a photon, the hole in the valence band may transfer to the hole-conducting MEH-PPV, and the electron can either remain in the quantum dot or move through the nanocrystal network by hopping or tunnelling. Depending on the polarity of the built-in and/or applied field, the electron and hole can move towards the ITO or towards the magnesium. When the electron moves to the ITO side, it will see a higher barrier by the tilted band

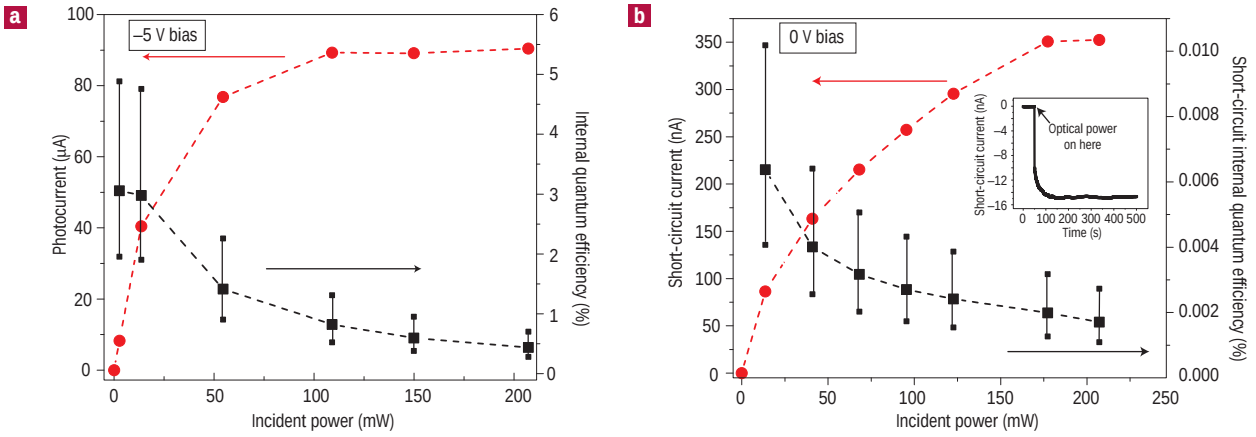

Figure 2 **Photocurrent and internal quantum efficiency versus incident optical power**. **a**, The photocurrent in red (circles) on the left axis and the internal quantum efficiency (squares) in black on the right axis are shown as a function of incident power at –5 V bias. **b**, Main panel: short-circuit current (circles) and corresponding internal quantum efficiency (squares) as a function of incident power. The lines are merely provided to guide the eye. Inset: stability of the short-circuit current as a function of time for a sample with much lower photovoltaic response than in Fig. 1b.

and PPV (ionization energy ~5.1 eV and electronic affinity ~2.7 eV; ref. 19) than when moving to the magnesium electrode. When the hole moves to the ITO, it also faces a barrier between MEH-PPV and PPV, and no barrier if it moves to the magnesium side. Reverse bias results in photogenerated holes being extracted through the ITO/PPV side of the sample, whereas forward bias results in electrons being extracted through that side. Thus, the higher photocurrent in the reverse bias suggests that the electron barrier posed by the PPV may be more severe than the hole barrier in carrier extraction.

Figure 1b shows dark and illuminated *I–V* curves for the region near 0 V, demonstrating the presence of a photovoltaic effect under continuous-wave illumination at 975 nm. The maximum short-circuit current is 350 nA for an incident power of 207 mW. The open-circuit voltage is 0.36 V. The photovoltaic effect was checked for hysteresis effects to see whether slow charge reorganization alone could be the cause. A sample demonstrating much lower short-circuit current (~15 nA) than shown in Fig. 1b was used to provide more convincing evidence that, even with very low short-circuit currents, the effect is not simply an artefact of hysteresis. The inset of Fig. 2b shows the result of this test where the sample was held at zero bias and the short-circuit current monitored over 500 s: the signal was stable over this time span. Further evidence that the effect was not hysteresis-based was provided by performing voltage scans in both directions (forward bias to reverse bias and vice versa); the direction of scan had negligible effect on the photovoltaic response. Although this photovoltaic response, which allows separation of an electron–hole pair at zero applied bias, could be indicative of a type-II heterostructure between the PbS nanocrystals and MEH-PPV, the built-in field in the device under zero bias is significant and could also allow charge separation with a marginal type-I heterostructure.

Figure 2a presents the dependence of photocurrent and internal quantum efficiency on the incident power at –5 V bias. The internal quantum efficiency is defined as the ratio of the number of collected charges to the number of absorbed photons at the pump wavelength. The calculation of internal quantum efficiency using absorption values obtained in reflection mode, the handling of optical interference effects and the range bars on these efficiency values are described in detail in the Methods. The percentage absorption at the 975 nm wavelength used to obtain the main efficiency points in Fig. 2a and b was 12.7%; the upper and lower range bars represent upper and lower bounds obtained by consideration of multiple pass propagation through the active layer. From the figure it can be seen that the photocurrent does not increase linearly with incident power. Above ~50 mW, the photocurrent increases more slowly with increased power. In the low power region, the recombination of trapped electrons in the nanocrystal network with holes in the neighbouring polymer dominates. When more photons are absorbed at higher powers, bimolecular recombination between free holes and electrons occurs in addition to the recombination at electron trap centres[8]. The additional bimolecular recombination reduces the number of photo-excited carriers and, hence, lowers the internal quantum efficiency as shown in Fig. 2a. At an incident power of 2.7 mW the internal quantum efficiency is about 3% (external quantum efficiency of ~0.38%), whereas at 207 mW the internal quantum efficiency is reduced to about 0.4%. The short-circuit current and corresponding internal quantum efficiency is plotted in Fig. 2b, showing a maximum value of ~0.006% (short-circuit external quantum efficiency of ~0.0008%). These zero-bias internal quantum efficiencies are about 500 times lower than at –5 V and show similar signs of a roll-off caused by bimolecular recombination at higher powers. The short-circuit internal quantum efficiency is much lower than the best previous reports for CdSe nanocrystal-based systems where the trioctylphosphine oxide (TOPO) ligands were removed by treatment with pyridine; for samples with the TOPO ligands still present on the nanocrystal surface, these systems showed internal quantum efficiencies closer to, but still slightly higher than, that reported here[8,20]. Further efforts are required in the PbS system to remove the ligands, as this could markedly improve efficiencies (especially in photovoltaic mode) in our system.

The 3% internal quantum efficiency at –5 V is an increase of three orders of magnitude over that reported previously[12] and is attributed principally to an improvement in film quality across these large-area devices. The MEH-PPV in previous work was typically cast from toluene and was not ultrasonicated or filtered. In the present work, the MEH-PPV was cast from chloroform, ultrasonicated for 1 hour before casting the films, and both the polymer and nanocrystal solutions were independently filtered. The combination of the above treatments was shown using atomic force microscopy to provide smoother films with fewer defects and pinholes than the previous process. The films produced as described previously[12] showed large centres of aggregated material and many pinholes; the newer films show much smaller regions of aggregated, transport-impeding material

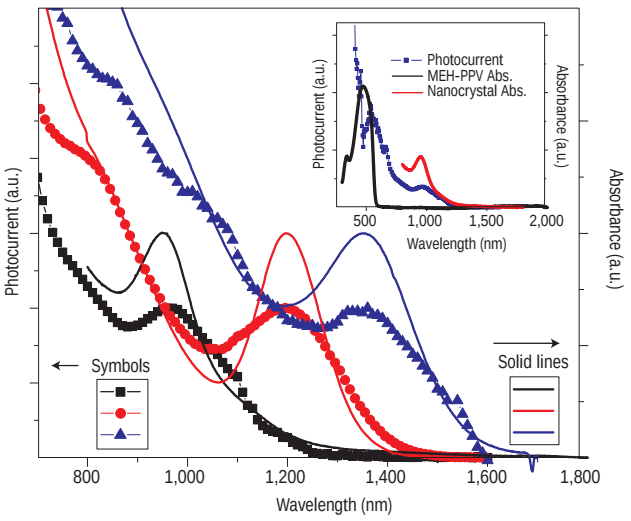

Figure 3 **Photocurrent spectral responses and absorption spectra**. Main panel: photocurrent spectral response (symbols) and the corresponding absorption spectra (solid line) for three different samples. The absorption peaks are tuned to 955 (black), 1,200 (red) and 1,355 nm (blue). Inset: extended spectral response for the sample centred at 955 nm, indicating the response in the region below ~600 nm where both the polymer and nanocrystal are excited. Also shown are the absorption spectra of the polymer and the nanocrystals.

and are pinhole-free. The improved surface of the films allows better interfacial contact with the upper metal electrode, resulting in better carrier extraction[21]. Films in the earlier work contained only ~60% nanocrystal by weight because higher loading gave films that suffered from excessive shorts. In this work, films containing 90% nanocrystal by weight were successfully cast by optimizing the concentration, and hence viscosity, of both the nanocrystal and polymer solutions. The increased nanocrystal loading probably resulted in improved electron transport. Pinholes previously[12] led to a photocurrent-to-dark-current ratio of ~10^{-4}, necessitating the use of lock-in techniques to detect the photocurrent signal. The present devices, with their orders-of-magnitude greater photocurrent-to-dark ratios and efficiencies, were readily studied using continuous-wave methods.

Figure 3 shows the absorbance spectrum of the nanocrystals (measured using a Varian CARY 500 Scan spectrophotometer) used in three different devices, each tuned to a different part of the infrared spectrum, and the measured photocurrent spectral response of each device. No bias was applied to the devices during measurement of the photocurrent spectrum, and the excitation was provided by narrow wavelength bands selected from a white light source by a monochromator. At wavelengths longer than 600 nm, the absorption of MEH-PPV is negligible; thus, all absorption at these wavelengths is assigned solely to the PbS nanocrystals. The absorption peaks at 955, 1,200 and 1,355 nm correspond to the first excitonic absorption features in the three different choices of PbS nanocrystals. The photocurrent spectra show peaks that match closely the absorption peaks associated with the nanocrystals. Along with demonstrating control over the spectral response, this result adds further evidence that the photocurrent is due to exciton formation in the nanocrystals followed by charge separation. The inset of Fig. 3 shows the spectral response of the device with the 955-nm response peak, including shorter wavelengths where the polymer is also excited. The photocurrent response peaks at a wavelength of 60 nm redshifted relative to the polymer absorption peak.

METHODS

PBS NANOCRYSTAL SYNTHESIS AND LIGAND EXCHANGE

The synthesis followed that used previously[13]. The as-prepared nanocrystals were capped with oleic acid ligands. A post-synthesis ligand exchange was performed to replace these with octylamine ligands. The original oleic-acid-capped nanocrystals were precipitated with methanol, dried and dispersed in an excess of octylamine. This solution was heated at 70 °C for ~16 hours. After heating, the octylamine capped nanocrystals were precipitated with N,N-dimethylformamide and redispersed in chloroform. The nanocrystals were then mixed with MEH-PPV to give a known weight fraction.

DEVICE PROCESSING

A 40 nm PPV hole transport layer was spin-coated on 2.5 × 2.5 cm^2 ITO-coated glass slide and annealed at 200 °C for 3 hours in vacuum to allow polymerization. A MEH-PPV/nanocrystal blend (90% nanocrystal by weight) dissolved in chloroform was spin-coated on the PPV layer to form a film of thickness 100–150 nm. Finally, the upper contact was deposited by vacuum evaporation forming a 3-mm^2 metal stack of 150 nm Mg/100 nm Ag/10 nm Au.

MEASUREMENT OF PHOTOCURRENT SPECTRAL RESPONSE

A bias of 0 V was applied to the sample connected in series with a load resistor of ~100 Ω, which was about three orders of magnitude smaller than the resistance of the sample. Illumination was provided by a white light source dispersed by a monochromator (Triax 320) and mechanically chopped at a frequency of ~250 Hz. Various filters were used to avoid overtones of the monochromator's grating from illuminating the sample. The potential drop across the load resistor was read by a lock-in amplifier (model SR803 DSP). The light intensity at each wavelength was separately measured. Then, the photocurrent at each wavelength was scaled to the same incident light intensity by assuming that the photocurrent was linearly proportional to the light intensity in the low-intensity region used.

CALCULATION OF INTERNAL QUANTUM EFFICIENCY

The percentage absorption used in the internal quantum efficiency calculation needs to account for the device structure, which creates multiple optical passes because of the mirror-like upper metallic contact. Hence, optical interference effects must be considered[22]. Two separate approaches were taken and the results compared. First, the device's absorption was directly measured in reflection mode (see Supplementary Information, Fig. S1). For the second method, the single-pass absorption was measured and scaled by a factor determined by the intensity increase created by interference. Using a multilayer program, it was determined that the maximum enhancement would be between 2 and 2.5 depending on the exact layer thickness and index of refraction of each layer. Because there is considerable uncertainty in these values we chose the more severe absorption enhancement factor of 2.5 to provide a conservative lower bound on efficiency. The single-pass absorption was used as the lower bound on absorption (upper bound on efficiency) to represent that case where negligible Fabry–Perot enhancement occurs. The intermediate efficiency points in Fig. 2 were obtained using the measured multi-pass absorption at 975 nm (12.7%), and the upper and lower bounds were obtained using the single-pass absorption at 975 nm (7.9%) and 2.5 enhancement absorption at 975 nm (19.8%), respectively.

Received 21 July 2004; accepted 19 November 2004; published 9 January 2005.

References

1. Forrest, S. R. The path to ubiquitous and low-cost organic electronic appliances on plastic. *Nature* **428,** 911–918 (2004).
2. Brabec, C. J. *et al.* A low-bandgap semiconducting polymer for photovoltaic devices and infrared diodes. *Adv. Funct. Mater.* **12,** 709–712 (2002).
3. Yoshino, K. *et al.* Near IR and UV enhanced photoresponse of C_{60}-doped semiconducting polymer photodiode. *Adv. Mater.* **11,** 1382–1385 (1999).
4. Huynh, W. U., Dittmer, J. J. & Alivisatos, A. P. Hybrid nanorod-polymer solar cells. *Science* **295,** 2425–2427 (2002).
5. Wang, Y. & Herron, N. Photoconductivity of CdS nanocluster-doped polymers. *Chem. Phys. Lett.* **200,** 71–75 (1992).
6. Dabbousi, B. O., Bawendi, M. G., Onitsuka, O. & Rubner, M. F. Electroluminescence from CdSe quantum-dot/polymer composites. *Appl. Phys. Lett.* **66,** 1316–1318 (1995).
7. Mattoussi, H. *et al.* Electroluminescence from heterostructures of poly(phenylene vinylene) and inorganic CdSe nanocrystals. *J. Appl. Phys.* **83,** 7965–7947 (1998).
8. Greenham, N. C., Peng, X. & Alivisatos, A. P. Charge separation and transport in conjugated-polymer/semiconductor-nanocrystal composites studied by photoluminescence quenching and photoconductivity. *Phys. Rev. B* **54,** 17628–17637 (1996).
9. Bakueva, L. *et al.* Size-tunable infrared (1000–1600 nm) electroluminescence from PbS quantum-dot nanocrystals in a semiconducting polymer. *Appl. Phys. Lett.* **82,** 2895–2897 (2003).
10. Tessler, N., Medvedev, V., Kazes, M., Kan, S. & Banin, U. Efficient near-infrared polymer nanocrystal light-emitting diodes. *Science* **295,** 1506–1508 (2002).
11. Steckel, J. S., Coe-Sullivan, S., Bulovic, V. & Bawendi, M. 1.3 μm to 1.55 μm tunable electroluminescence from PbSe quantum dots embedded within an organic device. *Adv. Mater.* **15,** 1862–1866 (2003).
12. McDonald, S. A., Cyr, P. W., Levina, L. & Sargent, E. H. Photoconductivity from PbS-nanocrystal/semiconducting polymer composites for solution-processible, quantum-size tunable infrared photodetectors. *Appl. Phys. Lett.* **85,** 2089–2091 (2004).
13. Hines, M. A. & Scholes, G. D. Colloidal PbS nanocrystals with size-tunable near-infrared emission: observation of post-synthesis self-narrowing of the particle size distribution. *Adv. Mater.* **15,** 1844–1849 (2003).
14. Skotheim, T. A. (ed.) *Handbook of Conducting Polymers* (Dekker, New York, 1986).
15. Greenwald, Y. *et al.* Polymer–polymer rectifying heterojunction based on poly(3,4-dicyanothiophene) and MEH-PPV. *J. Polym. Sci. A* **36,** 3115–3120 (1998).
16. Jin, S.-H. *et al.* Synthesis and characterization of highly luminescent asymmetric poly(p-phenylene vinylene) derivatives for light-emitting diodes. *Chem. Mater.* **14,** 643–650 (2002).
17. Greczynski, G., Kugler, Th. & Salaneck, W. R. Energy level alignment in organic-based three-layer structures studied by photoelectron spectroscopy. *J. Appl. Phys.* **88,** 7187–7191 (2000).

18. Brabec, C. J. *et al.* Origin of the open circuit voltage of plastic solar cells. *Adv. Funct. Mater.* **11,** 374–380 (2001).
19. Schlamp, M. C., Peng, X. & Alivisatos, A. P. Improved efficiencies in light emitting diodes made with CdSe(CdS) core/shell type nanocrystals and a semiconducting polymer. *J. Appl. Phys.* **82,** 5837–5842 (1997).
20. Ginger, D. S. & Greenham, N. C. Charge injection and transport in films of CdSe nanocrystals. *J. Appl. Phys.* **87,** 1361–1368 (2000).
21. Nguyen, T.-Q., Kwong, R. C., Thompson, M. E. & Schwartz, B. J. Improving the performance of conjugated polymer-based devices by control of interchain interactions and polymer film morphology. *Appl. Phys. Lett.* **76,** 2454–2456 (2000).
22. Peumans, P., Yakimov, A. & Forrest, S. R. Small molecular weight organic thin-film photodetectors and solar cells. *J. Appl. Phys.* **93,** 3693–3723 (2003).

Acknowledgements

We thank S. Hoogland for discussions and the following for support: the Government of Ontario through the Ontario Graduate Scholarships program (S.A.M.); Materials and Manufacturing Ontario, a division of the Ontario Centres of Excellence; the Natural Sciences and Engineering Research Council of Canada through its Collaborative Research and Development Program; Nortel Networks; the Canada Foundation for Innovation; the Ontario Innovation Trust; and the Canada Research Chairs Programme. Correspondence and requests for materials should be addressed to E.H.S.
Supplementary Information accompanies the paper on www.nature.com/naturematerials.

Competing financial interests

The authors declare that they have no competing financial interests.

Supplementary Figure – Edward H. Sargent